Astrodynamics Vol. 6, No. 4, 429–439, 2022 https://doi.org/10.1007/s42064-022-0145-1

Probe lifetime around natural satellites with obliquity

Marco Cinelli[1], Hanlun Lei[2], Emiliano Ortore[3](✉), and Christian Circi[4]

1. *Istituto di Astrofisica e Planetologia Spaziali (IAPS), Istituto Nazionale di Astrofisica (INAF), Roma 00133, Italy*
2. *School of Astronomy and Space Science and Key Laboratory of Modern Astronomy and Astrophysics, Ministry of Education, Nanjing University, Nanjing 210046, China*
3. *School of Aerospace Engineering, Sapienza University of Rome, Rome 00138, Italy*
4. *Department of Astronautical, Electrical, and Energy Engineering, Sapienza University of Rome, Rome 00138, Italy*

ABSTRACT

The dynamics of a probe orbiting a moon can be significantly influenced by the non-coincidence between the moon's equatorial and orbital planes. Thus, we performed a general analysis about the effects of the angle (obliquity) between the above-mentioned planes and of the angle (nodal phasing) between the nodal lines of the mother planet's apparent orbit and the probe orbit on the lifetime of the probe. The lifetime, strictly correlated to the variations in eccentricity of the probe orbit, was evaluated starting from low values of the semi-major axis, moderate eccentricity, and high inclination to offer high ground spatial resolution and extend latitudinal coverage of the natural satellite. This investigation, carried out through numerical simulations, may be useful for identifying the optimal initial conditions of the probe's orbit elements, leading to an important increase in the probe lifetime in missions devoted to the exploration of natural satellites.

KEYWORDS

third-body effect
natural satellite
probe lifetime

Research Article

Received: 19 April 2022
Accepted: 20 May 2022

1 Introduction

It is well known that the long-term dynamics of a probe moving around a natural satellite can be studied by performing a double average of the disturbing function. This function is written by considering the main perturbing effects acting on the probe, usually represented by the gravitational attraction of the planet around which the moon orbits (third-body effect), also called the mother planet (hereafter referred to as MP), and the principal gravitational asymmetries of the natural satellite (primary body). This approach, which can retain the "leading terms" related to the variations of the probe orbit elements, can be applied under the hypothesis that these orbit elements remain constant over the time intervals in which the aforementioned averages are taken (the orbital period of the probe and orbital period of the MP in its relative motion with respect to the natural satellite). Such a hypothesis is usually verified with a good level of accuracy, and consequently, the double-averaged approach enables an accurate estimation of the real dynamics of the probe. Concerning this, de Almeida Prado [1] and Broucke [2] described the equations related to the long-term dynamics of a probe under the third-body effect in the case of a circular orbit for the perturbing body. Domingos *et al.* [3] generalized the same issue to the case of an elliptical orbit for the perturbing body.

However, in the case of probes positioned over high-altitude orbits around moons (although very far from the MP, thus defining a hierarchical triple system) with a very massive MP (such as Jupiter or Saturn), the third-body perturbation can be strong enough to increase the amplitude of the periodic oscillations of the orbit elements (short-term effects) that are linked to the instantaneous position of the MP and averaged out (over the third-body period). In this case, the hypothesis assuming that the probe orbit elements are constant can induce non-negligible errors in predicting the real dynamics of the probe, and it is necessary to appropriately modify the classical double-averaged approach [4].

Most of the main moons of the solar system (e.g., Io,

✉ emiliano.ortore@uniroma1.it

Europa, Ganymede, Callisto, Titan, and Enceladus) are characterized by an MP that, in its relative motion with respect to the moon, quasi-lays on the moon's equatorial plane. This implies that the dynamics of the probe is not significantly influenced by the difference between the right ascension of the ascending node (RAAN) of the probe orbit and that of the disturbing body orbit [5], hereafter referred to as nodal phasing. Therefore, in many studies focused on the dynamical properties of a probe orbiting these natural satellites, the hypothesis of co-planarity between the orbital plane of the MP and the moon's equatorial plane has been adopted, thus neglecting the effect of nodal phasing (e.g., Refs. [6–9]). However, around natural satellites that do not have an orbital plane coinciding with their equatorial plane, the effects of this non-co-planarity (obliquity and nodal phasing) on the dynamics of the probe become important [10, 11].

In particular, the lifetime of a probe is critical in missions focused on natural satellites because of possible probe–moon collision. In fact, this element is strictly linked to the variation in the probe's orbit eccentricity due to gravitational attraction of the MP. Thus, the aim of this study is to investigate the influence of obliquity and nodal phasing on the lifetime of a probe orbiting at low altitude (to allow high ground spatial resolution of remotely sensed images) and high inclination (to gain wide latitudinal coverage of the moon) around a natural satellite. The work is organized as follows: Section 2 describes the averaging processes that lead to equations describing the long-term dynamics of a probe under the third-body effect, in the general case of an inclined elliptical orbit for the MP; Section 3 investigates the lifetime of the probe in this general case; and Section 4 summarizes the results of this study.

2 Long-term dynamics under the effect of a distant MP

Let us consider a hierarchical triple system formed by a probe, a natural satellite (moon), and its MP. The probe moves around the moon (primary body), which in turn orbits around the MP (disturbing body). For this system, the relative motions of the probe and MP with respect to the moon can be studied in a right-handed X, Y, Z reference system with its origin in the center of mass of the moon, Z axis coincident with the polar axis of the moon, and X and Y pointing in fixed directions on the equatorial plane of the moon. In particular, the X-axis is taken as coincident with the nodal line of the MP orbit so that the RAAN of the MP orbit ($\Omega_{\rm d}$), assumed to be constant, is equal to zero (Fig. 1).

This hypothesis is well verified, considering that the operational life of a probe around a natural satellite is usually far smaller than the rotational period of the nodal line of the perturbing body. Consequently, hereafter, the nodal phasing is intended to be $\Delta\Omega = \Omega - \Omega_{\rm d} = \Omega$, with Ω = RAAN of the probe orbit (angle, measured in the equatorial plane of the moon, between the X-axis and the nodal line of the probe orbit). In this reference system, assuming $\mu_{\rm d}$ as the planetary constant of the MP and S as the angle between the position vector of the probe

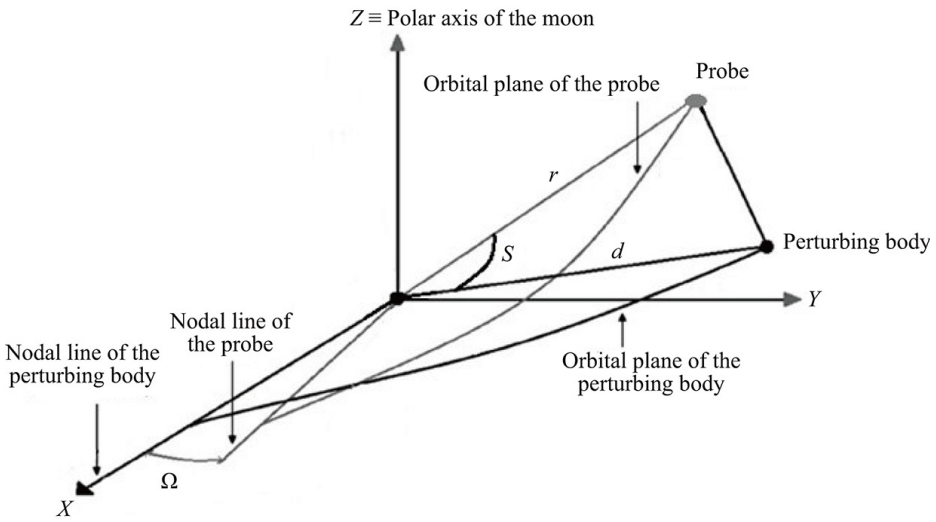

Fig. 1 Reference frame with origin in the center of mass of the moon.

and the position vector of the MP, two hypotheses are assumed:

- the MP orbit is outer with respect to the probe orbit;
- the probe–moon distance (r) is far less than the MP-moon distance (d), so that the traditional expansion in Legendre polynomials can be truncated at second order.

Then, the disturbing function (U_d) owing to the gravitational attraction of the MP can be written as

$$U_\mathrm{d} = \frac{\mu_\mathrm{d}}{d}\left(\frac{r}{d}\right)^2 \frac{3\cos^2 S - 1}{2} \tag{1}$$

with

$$\begin{aligned}\cos S = {} & \cos f(g_1 \cos f_\mathrm{d} + g_2 \sin f_\mathrm{d}) \\ & + \sin f(g_3 \cos f_\mathrm{d} + g_4 \sin f_\mathrm{d})\end{aligned} \tag{2}$$

In Eq. (2), f and f_d are the true anomalies of the probe and MP, respectively, and

$$\begin{aligned}g_1 = {} & \sin\omega[\cos i(\cos i_\mathrm{d}\cos\Omega\sin\omega_\mathrm{d} - \sin\Omega\cos\omega_\mathrm{d}) \\ & + \sin i_\mathrm{d}\sin i\sin\omega_\mathrm{d}] \\ & + \cos\omega(\cos i_\mathrm{d}\sin\Omega\sin\omega_\mathrm{d} + \cos\Omega\cos\omega_\mathrm{d}) \\ g_2 = {} & \cos\omega_\mathrm{d}(\cos i_\mathrm{d}\cos\omega\sin\Omega + \sin i_\mathrm{d}\sin i\sin\omega) \\ & + \cos i\sin\omega(\cos i_\mathrm{d}\cos\Omega\cos\omega_\mathrm{d} + \sin\Omega\sin\omega_\mathrm{d}) \\ & - \cos\omega\cos\Omega\sin\omega_\mathrm{d} \\ g_3 = {} & \cos i_\mathrm{d}\sin\omega_\mathrm{d}(\cos i\cos\omega\cos\Omega - \sin\omega\sin\Omega) \\ & + \sin i_\mathrm{d}\sin i\cos\omega\sin\omega_\mathrm{d} \\ & - \cos\omega_\mathrm{d}(\cos i\cos\omega\sin\Omega + \sin\omega\cos\Omega) \\ g_4 = {} & \sin\omega(\cos\Omega\sin\omega_\mathrm{d} - \cos i_\mathrm{d}\sin\Omega\cos\omega_\mathrm{d}) \\ & + \cos i\cos\omega(\cos i_\mathrm{d}\cos\Omega\cos\omega_\mathrm{d} + \sin\Omega\sin\omega_\mathrm{d}) \\ & + \sin i_\mathrm{d}\sin i\cos\omega\cos\omega_\mathrm{d}\end{aligned}$$

where ω and ω_d are the arguments of the pericenter of the orbits of the probe and MP, respectively; and i and i_d are the inclinations of the orbits of the probe and MP, respectively. The long-term dynamics of the probe under the third-body effect can be highlighted by first performing an average of Eq. (1) with respect to the positions of both the probe (over its orbital period) and MP (over the orbital period of the MP in its apparent motion with respect to the moon), then introducing this double-averaged potential into the Lagrange planetary equations (LPE). The first average, performed with respect to the orbital period of the probe (T), can be solved analytically using the eccentric anomaly of the probe (E). To this end, we use the following relationships:

$$r = a(1 - e\cos E)$$

$$\sin f = \frac{\sqrt{1-e^2}\sin E}{1 - e\cos E}$$

$$\cos f = \frac{\cos E - e}{1 - e\cos E}$$

to express Eq. (1) as a function of E, and thus we obtain

$$\begin{aligned}\langle U_\mathrm{d}\rangle = {} & \frac{1}{T}\int_0^\mathrm{T} U_\mathrm{d}\mathrm{d}t = \frac{1}{2\pi}\int_0^{2\pi} U_\mathrm{d}\mathrm{d}M \\ = {} & \frac{1}{2\pi}\int_0^{2\pi}(1 - e\cos E)U_\mathrm{d}\mathrm{d}E \\ = {} & -\frac{a^2\mu_\mathrm{d}(1 + e_\mathrm{d}\cos f_\mathrm{d})^3}{8a_\mathrm{d}^3(e_\mathrm{d}^2 - 1)^3}\Big\{3\cos(2f_\mathrm{d})[(1+4e^2)g_1^2 \\ & + (1-4e^2)g_2^2 + (1-e^2)(g_3^2 - g_4^2)] \\ & + 6\sin(2f_\mathrm{d})[g_1g_2(1+4e^2) + (1-e^2)g_3g_4] \\ & + 3e^2(4g_1^2 + 4g_2^2 - g_3^2 - g_4^2 - 2) + 3g_1^2 \\ & + 3g_2^2 + 3g_3^2 + 3g_4^2 - 4\Big\}\end{aligned} \tag{3}$$

where a and a_d are the semi-major axes of the orbits of the probe and MP, respectively; e and e_d are the eccentricities of the orbits of the probe and MP, respectively; and M is the mean anomaly of the probe. The second average, performed with respect to the orbital period of the MP (T_d), can be computed analytically by considering the true anomaly of the MP. In this case, we have

$$\begin{aligned}\langle\langle U_\mathrm{d}\rangle\rangle = {} & \frac{1}{T_\mathrm{d}}\int_0^{T_\mathrm{d}}\langle U_\mathrm{d}\rangle\mathrm{d}t = \frac{1}{2\pi}\int_0^{2\pi}\langle U_\mathrm{d}\rangle\mathrm{d}M_\mathrm{d} \\ = {} & \frac{1}{2\pi}\int_0^{2\pi}\frac{(1-e_\mathrm{d}^2)^{3/2}}{(1 + e_\mathrm{d}\cos f_\mathrm{d})^2}\langle U_\mathrm{d}\rangle\mathrm{d}f_\mathrm{d} \\ = {} & \frac{a^2\mu_\mathrm{d}}{8a_\mathrm{d}^3(1-e_\mathrm{d}^2)^{3/2}}[(3g_1^2 + 3g_2^2 + 3g_3^2 + 3g_4^2 - 4) \\ & + 3e^2(4g_1^2 + 4g_2^2 - g_3^2 - g_4^2 - 2)]\end{aligned} \tag{4}$$

where M_d denotes the mean anomaly of MP. Equation (4) indicates that the double-averaged disturbing function is composed of a part that is independent of the eccentricity of the probe and a part that depends on e^2. By replacing Eq. (4) in the LPE, the equations governing the long-term variations of eccentricity, inclination, RAAN, and argument of the pericenter of the probe orbit can be expressed as Eq. (5):

$$\begin{aligned}\dot{e} = {} & -\frac{15}{16}\frac{\mu_\mathrm{d}}{a_\mathrm{d}^3(1-e_\mathrm{d}^2)^{3/2}}\frac{e\sqrt{1-e^2}}{n}\sin(2\omega) \\ & \cdot\Big[2\cot(2\omega)(\sin(2i_\mathrm{d})\sin i\sin\Omega - \sin^2 i_\mathrm{d}\cos i\sin(2\Omega)) \\ & + 2\cos^2\Omega(\cos^2 i_\mathrm{d}\cos^2 i - 1) + \sin^2\Omega(\cos(2i)\end{aligned}$$

$$
\begin{aligned}
&- \cos(2i_{\mathrm{d}})) + \sin(2i_{\mathrm{d}})\sin(2i)\cos\Omega + 2\sin^2 i_{\mathrm{d}}\sin^2 i\Big] \\
\dot{i} &= \frac{3}{8}\frac{\mu_{\mathrm{d}}}{a_{\mathrm{d}}^3\sqrt{1-e^2}(1-e_{\mathrm{d}}^2)^{3/2}n} \\
&\cdot(\sin i_{\mathrm{d}}\sin i\cos\Omega + \cos i_{\mathrm{d}}\cos i) \\
&\cdot\Big[\sin i_{\mathrm{d}}\sin\Omega(5e^2\cos(2\omega) + 3e^2 + 2) \\
&+ 5e^2\sin(2\omega)(\sin i_{\mathrm{d}}\cos i\cos\Omega - \cos i_{\mathrm{d}}\sin i)\Big] \\
\dot{\Omega} &= \frac{3\mu_{\mathrm{d}}}{32a_{\mathrm{d}}^3\sqrt{1-e^2}(1-e_{\mathrm{d}}^2)^{3/2}n} \\
&\cdot\Big[\cos i(5e^2\cos(2\omega) - 3e^2 - 2)(-2\sin^2 i_{\mathrm{d}}\cos(2\Omega) \\
&+ 3\cos(2i_{\mathrm{d}}) + 1) + 10e^2\sin(2\omega)(\sin^2 i_{\mathrm{d}}\sin(2\Omega) \\
&+ \sin(2i_{\mathrm{d}})\cot i\sin\Omega) - 2\sin(2i_{\mathrm{d}})\cos(2i)\csc i\cos\Omega \\
&\cdot(5e^2\cos(2\omega) - 3e^2 - 2)\Big] \\
\dot{\omega} &= -\frac{3}{128}\frac{\mu_{\mathrm{d}}}{a_{\mathrm{d}}^3\sqrt{1-e^2}(1-e_{\mathrm{d}}^2)^{3/2}n} \\
&\cdot\Big\{4\sin^2 i_{\mathrm{d}}\cos(2\Omega)[5(2e^2-3)\cos(2\omega) + 6e^2 \\
&+ 10\cos(2i)\sin^2\omega - 1] \\
&+ 40(2-e^2)\sin^2 i_{\mathrm{d}}\cos i\sin(2\omega)\sin(2\Omega) \\
&- 20\sin(2i_{\mathrm{d}})\csc i\sin(2\omega)\sin\Omega \\
&\cdot[(e^2-2)\cos(2i) - 3e^2 + 2] \\
&- 4\sin(2i_{\mathrm{d}})\cot i\cos\Omega[2(e^2-1)(5\cos(2\omega) - 3) \\
&- 20\cos(2i)\sin^2\omega] \\
&+ 2[1 + 3\cos(2i_{\mathrm{d}})][5\cos(2\omega)(2e^2 + \cos(2i) - 1) \\
&- 2e^2 - 5\cos(2i) - 3]\Big\} \qquad (5)
\end{aligned}
$$

where n is the probe's mean motion and $\cot\alpha = 1/\tan\alpha = \cos\alpha/\sin\alpha$.

Equations (5) are mutually matched. By integrating this system of equations numerically, step by step, it is possible to determine the long-term variations of the probe orbit elements. Having averaged out the mean anomaly of the probe implies that the semi-major axis is constant, on average. This can easily be highlighted by observing the form of the LPE or, equivalently, by expressing the perturbation equations in the canonical form using the Delaunay elements.

When $i_{\mathrm{d}} = 0°$, the RAAN of the perturbing body is not defined, and the problem is axisymmetric with respect to the polar axis of the moon. The RAAN of the probe, which has no influence on its dynamics, represents a cyclic variable, leading to the conservation of its conjugate momentum, the Z-component of the angular momentum $\sqrt{\mu a(1-e^2)}\cos i = \text{constant}$ [2].

When the temporal evolution of the RAAN of the probe orbit is small in the time interval of interest, a fixed mean value for this orbit element may be considered in Eq. (5) to find a first-guess solution for the secular dynamics of the probe. Imposing the same condition (for example, $\Omega = 0$) in the disturbing function (Eq. (4)) would theoretically represent an approximation (that implies only a modification of the equation related to the variation in inclination). In fact, as pointed out by Naoz *et al.* [12], the elimination of the RAAN in the disturbing function (or in the Hamiltonian) would mean that the Z-component of the angular momentum of the probe is a constant, whereas this should occur only for $i_{\mathrm{d}} = 0°$.

3 Effects of the obliquity and nodal phasing

The lifetime of a probe is a key element of missions devoted to the observation of moons, and this element can be directly correlated to the evolution of the orbit eccentricity (as probe–moon collision occurs when the altitude of the pericenter of the probe orbit equals the radius of the moon). For this reason, we performed a numerical investigation into this issue, considering the general case of an inclined elliptical orbit for the MP (Eq. (5)) and adding the well-known secular variations of RAAN and ω due to the moon's oblateness (J_2 is the first zonal harmonic of the moon's gravitational field, and R_{P} is the mean equatorial radius of the moon):

$$
\begin{aligned}
\dot{e} &= -\frac{15}{16}\frac{\mu_{\mathrm{d}}}{a_{\mathrm{d}}^3(1-e_{\mathrm{d}}^2)^{3/2}}\frac{e\sqrt{1-e^2}}{n}\sin(2\omega) \\
&\cdot\Big[2\cot(2\omega)(\sin(2i_{\mathrm{d}})\sin i\sin\Omega - \sin^2 i_{\mathrm{d}}\cos i\sin(2\Omega)) \\
&+ 2\cos^2\Omega(\cos^2 i_{\mathrm{d}}\cos^2 i - 1) + \sin^2\Omega(\cos(2i) \\
&- \cos(2i_{\mathrm{d}})) + \sin(2i_{\mathrm{d}})\sin(2i)\cos\Omega + 2\sin^2 i_{\mathrm{d}}\sin^2 i\Big] \\
\dot{i} &= \frac{3}{8}\frac{\mu_{\mathrm{d}}}{a_{\mathrm{d}}^3\sqrt{1-e^2}(1-e_{\mathrm{d}}^2)^{3/2}n}
\end{aligned}
$$

$$\cdot (\sin i_{\mathrm{d}} \sin i \cos\Omega + \cos i_{\mathrm{d}} \cos i)$$
$$\cdot \Big[\sin i_{\mathrm{d}} \sin\Omega (5e^2 \cos(2\omega) + 3e^2 + 2)$$
$$+ 5e^2 \sin(2\omega)(\sin i_{\mathrm{d}} \cos i \cos\Omega - \cos i_{\mathrm{d}} \sin i) \Big]$$

$$\dot{\Omega} = \frac{3\mu_{\mathrm{d}}}{32 a_{\mathrm{d}}^3 \sqrt{1-e^2}(1-e_{\mathrm{d}}^2)^{3/2} n}$$
$$\cdot \Big[\cos i (5e^2 \cos(2\omega) - 3e^2 - 2)(-2\sin^2 i_{\mathrm{d}} \cos(2\Omega)$$
$$+ 3\cos(2i_{\mathrm{d}}) + 1) + 10e^2 \sin(2\omega)(\sin^2 i_{\mathrm{d}} \sin(2\Omega)$$
$$+ \sin(2i_{\mathrm{d}}) \cot i \sin\Omega) - 2\sin(2i_{\mathrm{d}}) \cos(2i) \csc i \cos\Omega$$
$$\cdot (5e^2 \cos(2\omega) - 3e^2 - 2) \Big] - \frac{3J_2 n R_{\mathrm{P}}^2}{2a^2(1-e^2)^2} \cos i$$

$$\dot{\omega} = -\frac{3}{128} \frac{\mu_{\mathrm{d}}}{a_{\mathrm{d}}^3 \sqrt{1-e^2}(1-e_{\mathrm{d}}^2)^{3/2} n}$$
$$\cdot \Big\{ 4\sin^2 i_{\mathrm{d}} \cos(2\Omega)[5(2e^2-3)\cos(2\omega) + 6e^2$$
$$+ 10\cos(2i)\sin^2\omega - 1]$$
$$+ 40(2-e^2)\sin^2 i_{\mathrm{d}} \cos i \sin(2\omega)\sin(2\Omega)$$
$$- 20\sin(2i_{\mathrm{d}}) \csc i \sin(2\omega)\sin\Omega$$
$$\cdot [(e^2-2)\cos(2i) - 3e^2 + 2]$$
$$- 4\sin(2i_{\mathrm{d}}) \cot i \cos\Omega [2(e^2-1)(5\cos(2\omega) - 3)$$
$$- 20\cos(2i)\sin^2(\omega)]$$
$$+ 2[1 + 3\cos(2i_{\mathrm{d}})][5\cos(2\omega)(2e^2 + \cos(2i) - 1)$$
$$- 2e^2 - 5\cos(2i) - 3] \Big\} + \frac{3J_2 n R_{\mathrm{P}}^2}{8a^2(1-e^2)^2}(5\cos(2i) + 3) \tag{6}$$

A broad range of numerical simulations have been executed considering the Jupiter–Europa system. Accordingly, Figs. 2–5 report the lifetime of a probe in a low-altitude and high-inclination orbit, obtained by integrating the system composed of Eq. (6). However, to generalize the results and provide references for practical applications, fictitious values for Jupiter's orbit inclination were also considered: $i_{\mathrm{d}} = 0°$ (Fig. 2, which is close to the real value); $i_{\mathrm{d}} = 30°$ (Fig. 3); $i_{\mathrm{d}} = 60°$ (Fig. 4); and $i_{\mathrm{d}} = 90°$ (Fig. 5). With regard to the probe orbit elements, the following initial conditions were implemented: $a = 1.1R_{\mathrm{P}}$, $e = 0.01$ and $i = 65°$, 75°, 85°, and 95°. Regarding the nodal phasing and the argument of the pericenter, the simulations were extended to their entire definition ranges (for all figures, $\Omega_{\mathrm{d}} = 0°$, so that $\Delta\Omega = \Omega$). For the other parameters involved, the following data provided by the Jet Propulsion Laboratory (JPL) of NASA [13] were implemented: $a_{\mathrm{d}} = 671{,}100$ km,

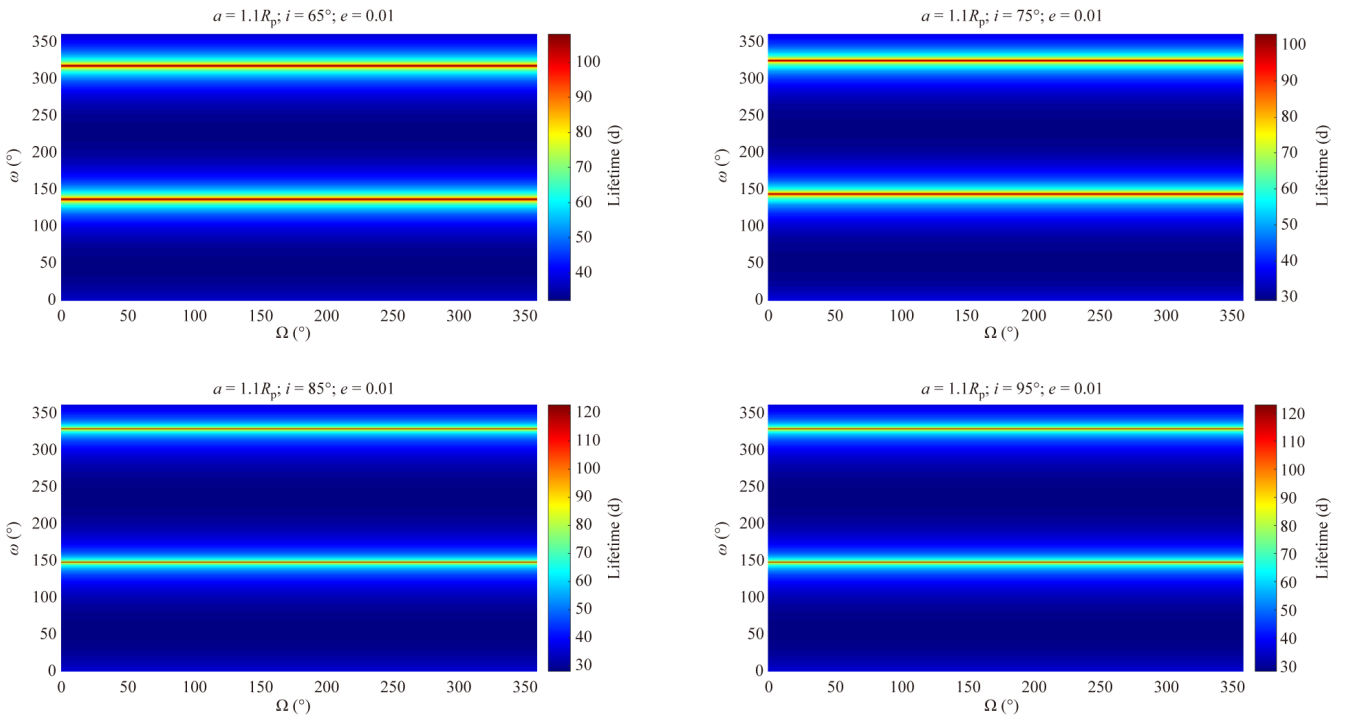

Fig. 2 Lifetime of a probe around Europa, assuming that Jupiter's relative orbit is on the equatorial plane of Europa.

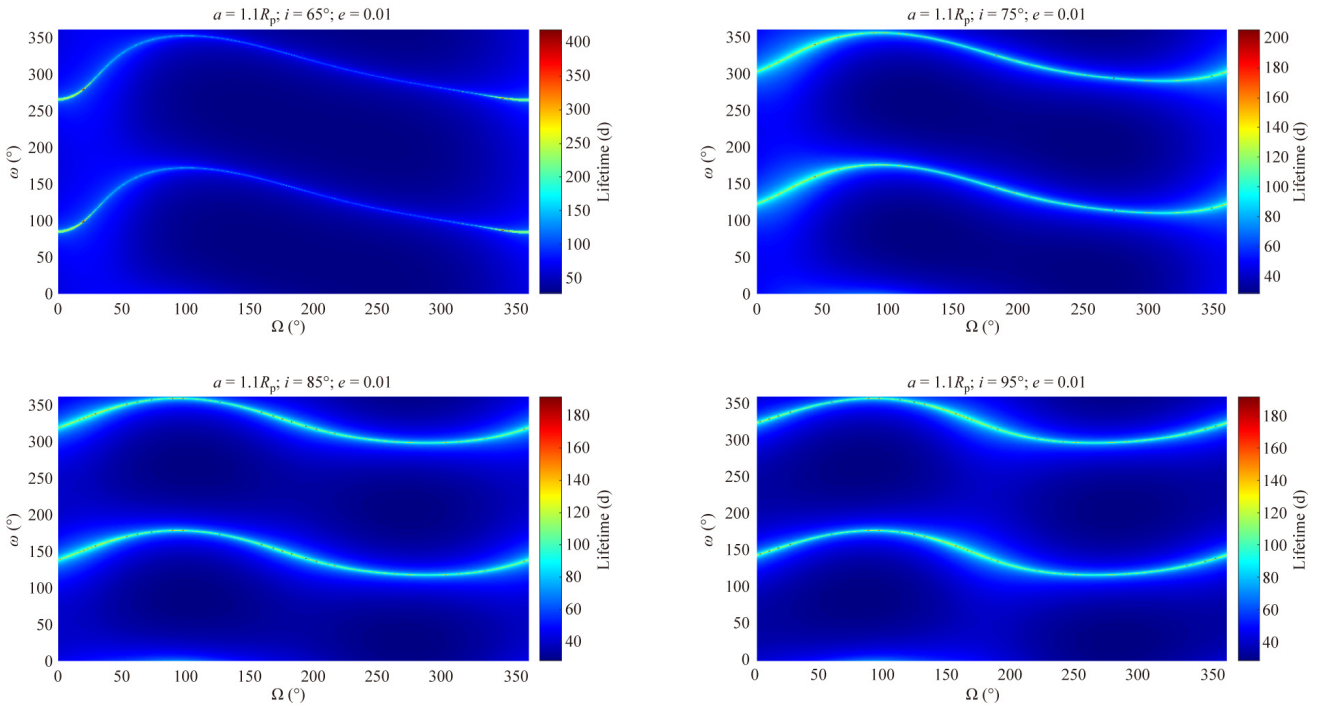

Fig. 3 Lifetime of a probe around Europa, taking a fictitious value of 30° as the inclination of Jupiter's relative orbit.

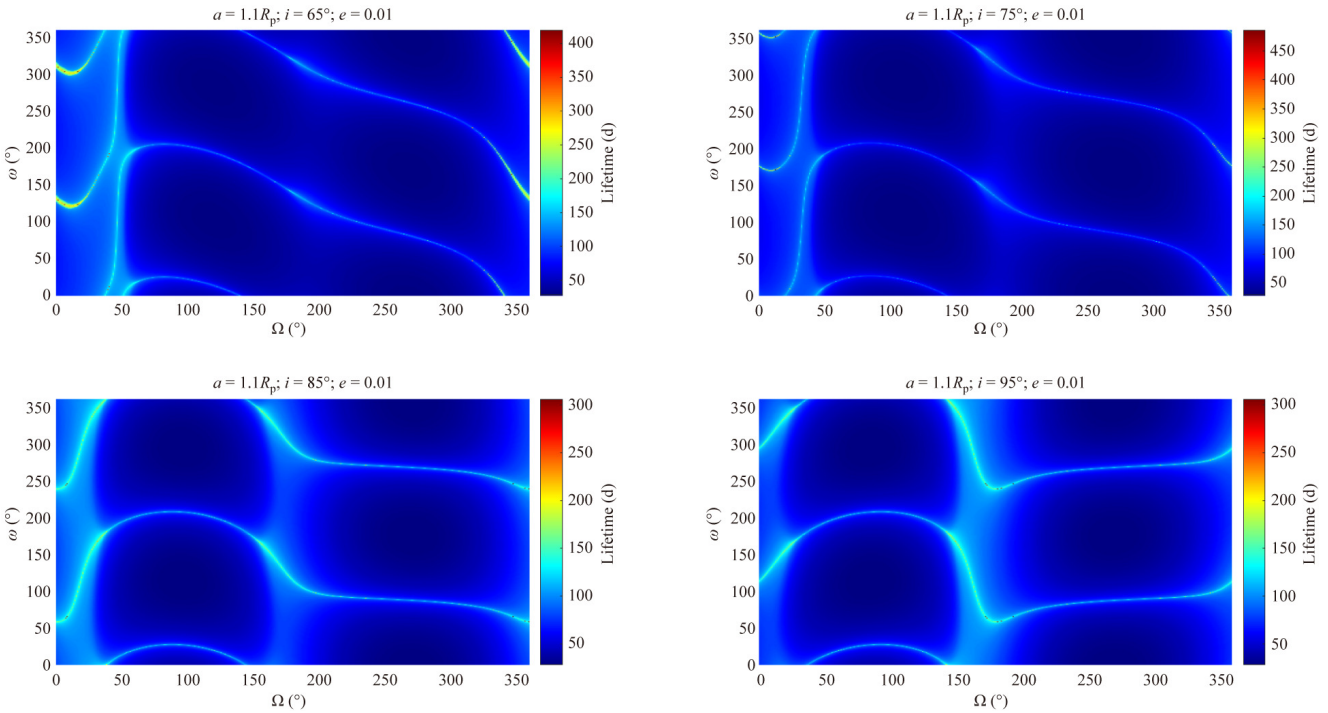

Fig. 4 Lifetime of a probe around Europa, taking a fictitious value of 60° as the inclination of Jupiter's relative orbit.

$e_d = 0.0094$, $\mu_d = 3{,}202.74$ km^3/s^2, $R_P = 1{,}560.8$ km, and $J_2 = 4.355\times10^{-4}$ (whose uncertainty is $\pm8.2\times10^{-6}$).

In Fig. 2 ($i_d = 0°$), the problem is axisymmetric and, consequently, the nodal phasing does not influence the probe's dynamics. Therefore, only the initial value of ω plays a key role in the probe lifetime. In particular, in each figure, two narrow strips of ω values are shown to provide the longest lifetime (120 terrestrial days). These

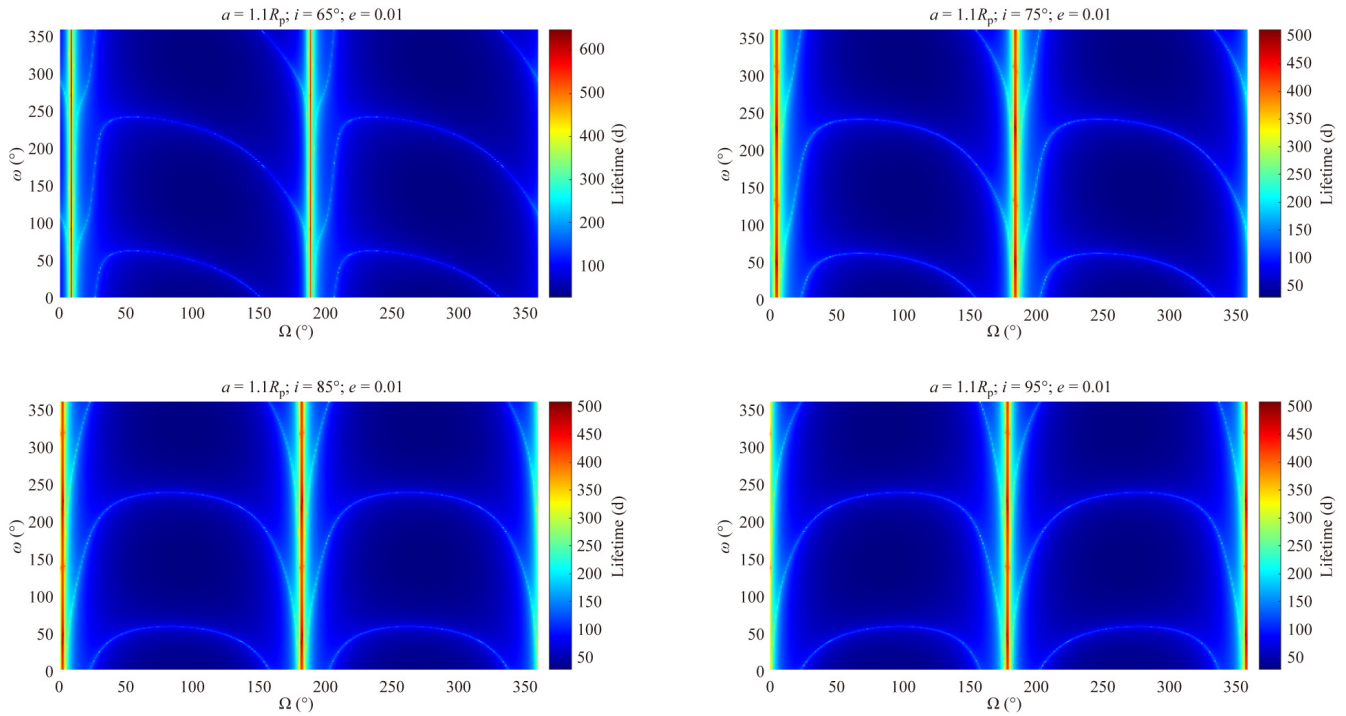

Fig. 5 Lifetime of a probe around Europa, taking a fictitious value of 90° as the inclination of Jupiter's relative orbit.

two strips are separated by an interval of 180° and are located around $\omega = 137°$ and 317° at $i = 65°$, $\omega = 145°$ and 325° at $i = 75°$, and $\omega = 147°$ and 327° at $i = 85°$ and 95°. The strips are horizontal, to highlight the non-influence of the nodal phasing, and become thinner as the probe's orbit inclination increases. Paskowitz and Scheeres [8] and Cinelli *et al.* [5] highlighted how the probe lifetime around Europa is strongly influenced by the initial value of the argument of the pericenter of the probe orbit. In particular, in Ref. [5], the two narrow strips were not perfectly horizontal, but oscillated around the values reported above as a function of the nodal phasing (Ω). This is because of the non-perfect co-planarity between Jupiter's relative orbit and Europa's equatorial plane, considered in that work. In the same work, the effect of the ellipticity of Europa equator was evaluated (C_{22} harmonic), showing how it increases the amplitude of the oscillations of the strips.

In Fig. 3 ($i_d = 30°$), the effect of nodal phasing becomes significant, and consequently, the narrow strips oscillate significantly as a function of Ω. In particular, at $i = 65°$, the strips oscillate over a wider range of values of ω and are more asymmetric with respect to the cases at higher inclination. The longest lifetime increases considerably with respect to the case at $i_d = 0°$, especially for $i = 65°$, where they exceed 400 terrestrial days.

In Fig. 4 ($i_d = 60°$), the influence of the nodal phasing is strong, and the strips are considerably asymmetric. At $i = 65°$ and 75°, for any ω, it is possible to find an appropriate value of Ω that maximizes the lifetime. The longest lifetime exceeds 300 terrestrial days. Vertical strips at high lifetime are also present (at approximately $\Omega = 0°$–30° and $\Omega = 150°$–180°) to highlight the important dependence on Ω.

In Fig. 5 ($i_d = 90°$), the longest lifetime is very high (over 500 terrestrial days), reaching a maximum for values of Ω around 0° and 180° (vertical strips). All cases present these two vertical strips. Considering the Jupiter–Europa system with $i_d = 90°$ and including the J_2 effect, Fig. 6 presents the case of $a = 1.2R_P$ and $e = 0.1$. Here, the strips are not perfectly vertical, and the longest lifetime is even longer than 5 terrestrial years.

The variation in eccentricity is directly correlated to the third-body perturbation (Eq. (5)), while the moon's oblateness, causing secular variations in RAAN and argument of pericenter, has an indirect effect on its temporal evolution. Thus, to highlight the contribution of the gravitational attraction of Jupiter to the probe lifetime, Europa's oblateness effect was also removed. Accordingly, Fig. 7 shows the lifetime obtained by

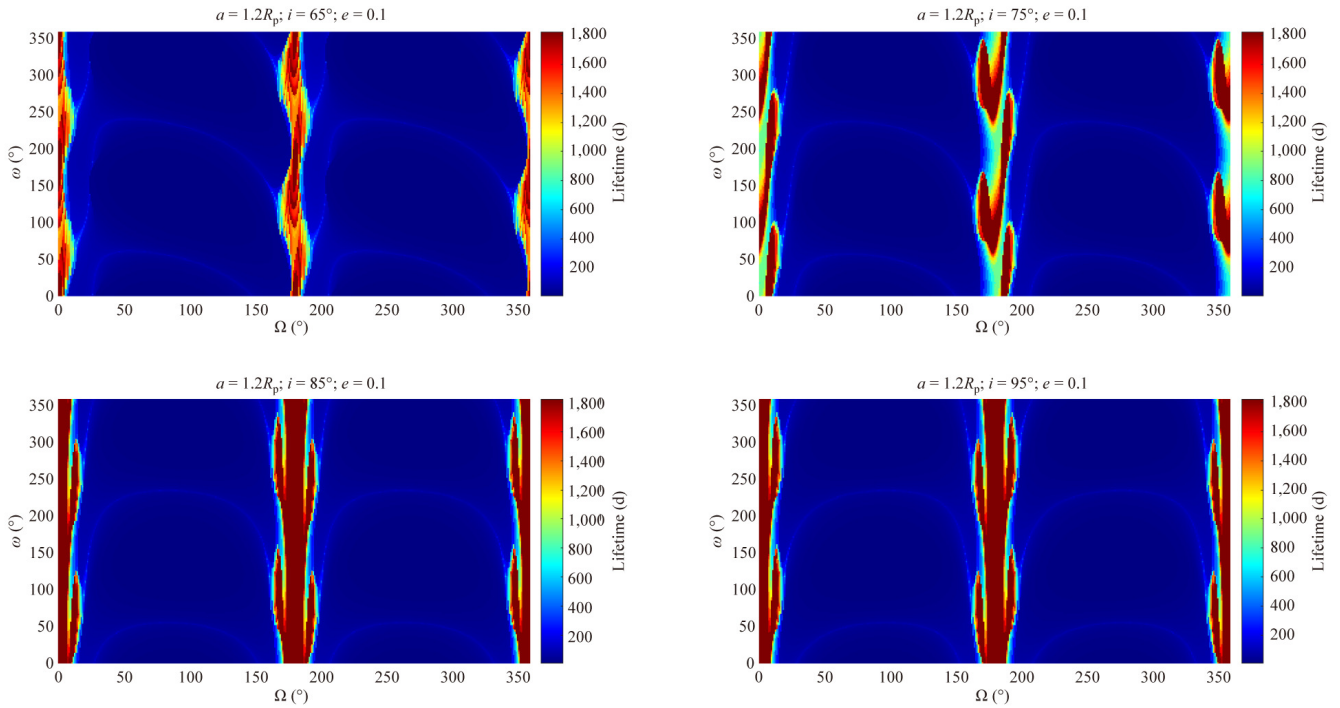

Fig. 6 Lifetime of a probe around Europa, taking a fictitious value of 90° for the inclination of Jupiter's relative orbit. The semi-major axis and eccentricity are higher than those in Figs. 2–5.

integrating the system of Eq. (5) and assuming the following initial conditions for the probe's orbit elements: $a = 1.1R_P$, $e = 0.01$, and $i = 95°$. As for the MP inclination, the upper-left plot refers to $i_d = 0°$, the upper-right plot refers to $i_d = 30°$, the lower-left plot to $i_d = 60°$, and the lower-right plot to $i_d = 90°$.

Similar to Fig. 2, in the case of $i_d = 0°$ in Fig. 7, there are two horizontal narrow strips, separated by an interval of 180°, that provide the longest lifetime (now located around $\omega = 143°$ and 323°). This case is related to the phase diagram shown in Fig. 2 in Ref. [2]. In this diagram, the level curves obtained by exploiting the two prime integrals of motion for this axisymmetric problem are reported (the disturbing function is constant in the averaged problem, and the Z-component of the angular momentum is constant). The values $\omega = 143°$ and 323° are, indeed, in the $(e\cos\omega, e\sin\omega)$ plane, very close to the dynamical separatrix that divides the diagram into libration and circulation regions for the argument of the pericenter. The same level curves can also be found in Fig. 1 in Ref. [14] (where the Mercury–Sun system was considered). In that work, the level curves were reported in the (e, ω) plane for $i = 90°$. The temporal evolutions of eccentricity and argument of the pericenter have also been described in Ref. [5], considering both the non-perfect co-planarity between Jupiter's relative orbit and Europa's equatorial plane, and the effects of the second-order and degree gravity field of Europa.

The results for $i_d = 0°$ and 30° in Fig. 7 (upper plots) are similar to those including the effect of Europa's oblateness, with the central values of the strips varying slightly. For $i_d = 60°$, the differences are more marked. In fact, the lifetime extends over almost five years, and a vertical strip appears around $\Omega = 180°$ (the other strips are not symmetric with respect to it). For $i_d = 90°$, the results are still similar to those with Europa's oblateness, but the lifetime is longer, and the strips around $\Omega = 0°$ and 180° are far larger. Additional numerical simulations were performed considering the Saturn–Enceladus system. The system of Eq. (6) was integrated, adopting fictitious values for the third-body inclination to generalize the results and provide references for real applications. For Enceladus, the data reported in Ref. [15] were used ($J_2 = 5.4352 \times 10^{-3}$). Figure 8 shows the results obtained starting from $a = 1.1R_P$, $e = 0.01$, and $i = 95°$. The upper-left plot refers to $i_d = 0°$ (approximately equal to the real value), the upper-right plot refers to $i_d = 30°$, the lower-left plot

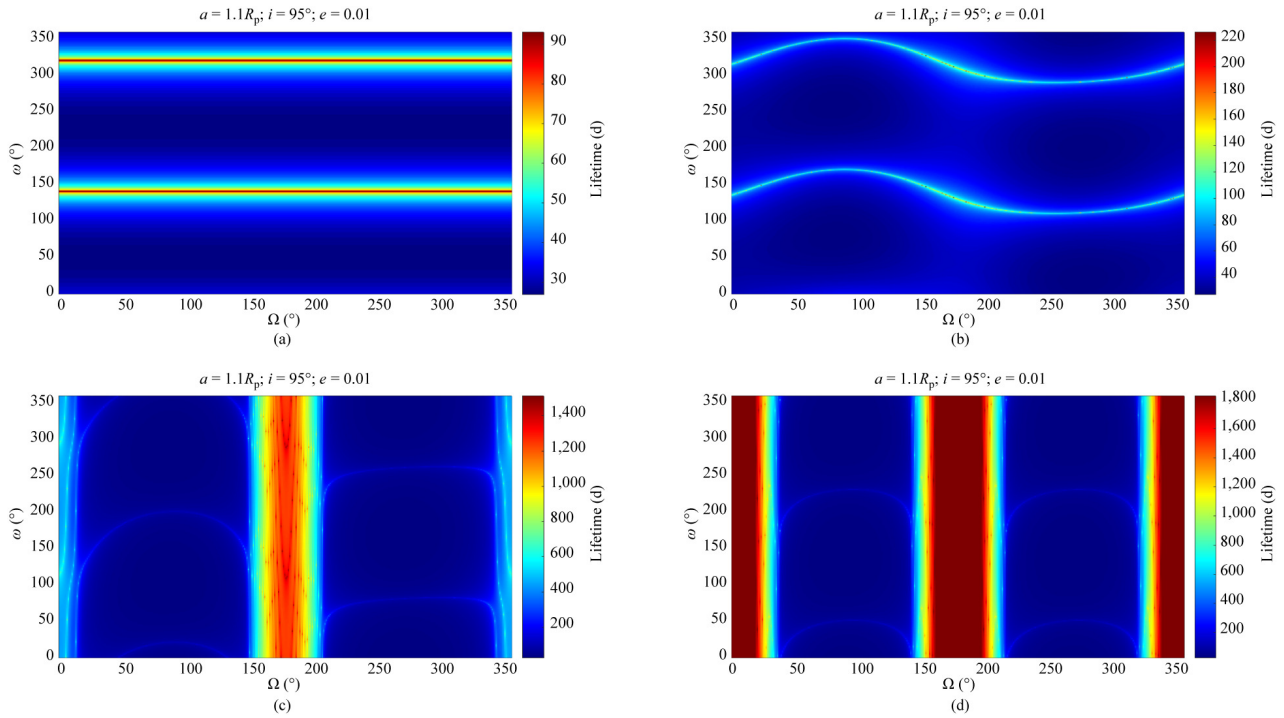

Fig. 7 Lifetime of a probe around Europa, assuming that i_d = (a) 0°, (b) 30°, (c) 60°, and (d) 90° for Jupiter. Europa's oblateness is neglected.

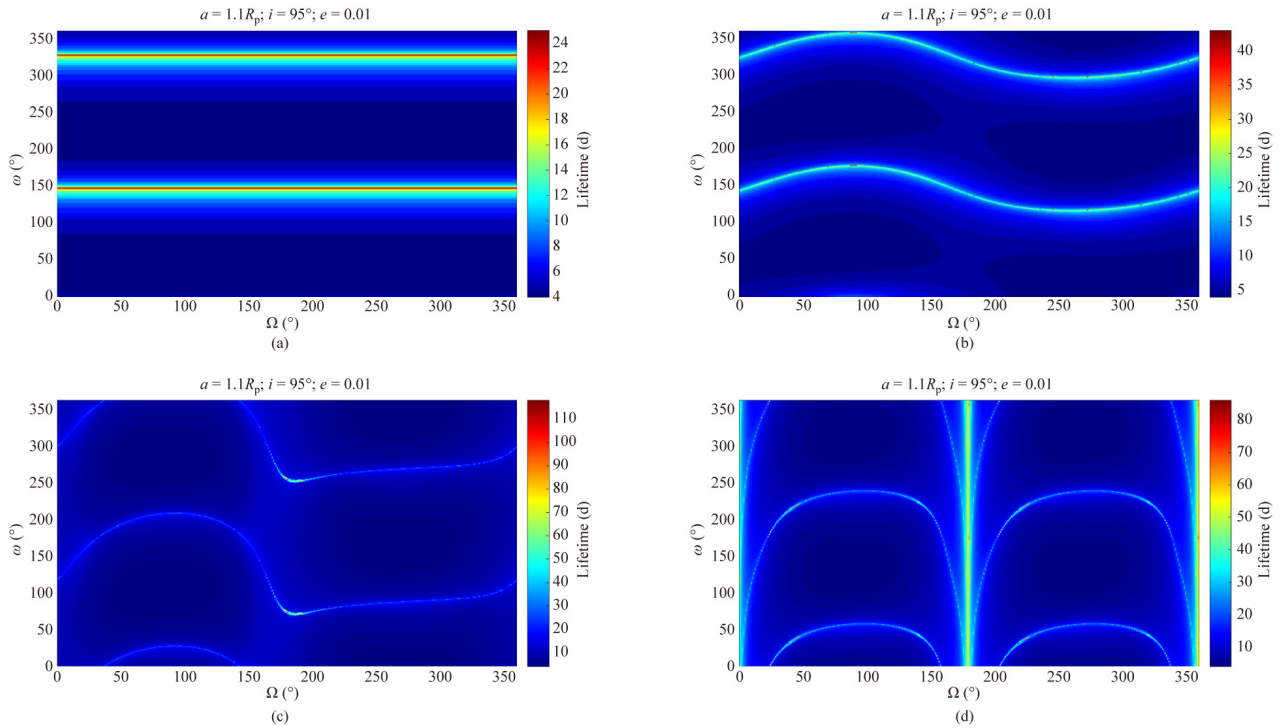

Fig. 8 Lifetime of a probe around Enceladus, assuming i_d = (a) 0°, (b) 30°, (c) 60°, and (d) 90° for Saturn.

refers to $i_d = 60°$, and the lower-right plot refers to $i_d = 90°$ (30°, 60°, and 90° are fictitious values).

As the evidence shows, although the lifetime is obviously different, from a dynamical point of view, the results are qualitatively the same as those related to the Jupiter–Europa system. In addition, note that, as

in the case of a probe orbiting Europa [5], inside all the horizontal and oscillating strips presented in this section, many specific values of Ω at the longest lifetime were obtained.

4 Conclusions

This study investigated the lifetime of a probe in a low-altitude and high-inclination orbit around a natural satellite. This issue was addressed by considering the moon's oblateness and the disturbing attraction of the mother planet in the gravity-gradient approximation (second-order approximation for the third-body disturbing function), considering the general case of an inclined elliptical orbit for the disturbing body. Numerical simulations highlighted how the lifetime of the probe is influenced by both the third-body inclination (obliquity) and the angle (nodal phasing) between the nodal lines of the mother planet and probe orbits. The influence of the nodal phasing is moderate for low inclinations (i_{d}) of the mother planet orbit, becoming significant at $i_{\mathrm{d}} = 30^\circ$ and strong at $i_{\mathrm{d}} = 60^\circ$ and over. In the (Ω, ω) plane, the longest lifetime is located inside strips, and the absolute maximum lifetime occurs when the mother planet's orbit is perpendicular to the equatorial plane of the natural satellite, with values of nodal phasing close to 0° and 180° (vertical strips).

Funding note

Open access funding provided by Sapienza University of Rome within the CRUI-CARE Agreement.

Declaration of competing interest

The authors have no competing interests to declare that are relevant to the content of this article.

References

[1] De Almeida Prado, A. F. B. Third-body perturbation in orbits around natural satellites. *Journal of Guidance, Control, and Dynamics*, **2003**, 26(1): 33–40.

[2] Broucke, R. A. Long-term third-body effects via double averaging. *Journal of Guidance, Control, and Dynamics*, **2003**, 26(1): 27–32.

[3] Domingos, R. C., de Moraes, R. V., de Almeida Prado, A. F. B. Third-body perturbation in the case of elliptic orbits for the disturbing body. *Mathematical Problems in Engineering*, **2008**: 763654.

[4] Lei, H. L., Circi, C., Ortore, E. Modified double-averaged Hamiltonian in hierarchical triple systems. *Monthly Notices of the Royal Astronomical Society*, **2018**, 481(4): 4602–4620.

[5] Cinelli, M., Ortore, E., Circi, C. Long lifetime orbits for the observation of Europa. *Journal of Guidance, Control, and Dynamics*, **2018**, 42(1): 123–135.

[6] Scheeres, D. J., Guman, M. D., Villac, B. F. Stability analysis of planetary satellite orbiters: Application to the Europa orbiter. *Journal of Guidance, Control, and Dynamics*, **2001**, 24(4): 778–787.

[7] Lara, M., Juan, J. F. S. Dynamic behavior of an orbiter around Europa. *Journal of Guidance, Control, and Dynamics*, **2005**, 28(2): 291–297.

[8] Paskowitz, M. E., Scheeres, D. J. Design of science orbits about planetary satellites: Application to Europa. *Journal of Guidance, Control, and Dynamics*, **2006**, 29(5): 1147–1158.

[9] Russell, R. P., Lara, M. On the design of an Enceladus science orbit. *Acta Astronautica*, **2009**, 65(1–2): 27–39.

[10] Liu, X. D., Baoyin, H. X., Ma, X. R. Long-term perturbations due to a disturbing body in elliptic inclined orbit. *Astrophysics and Space Science*, **2012**, 339(2): 295–304.

[11] Nie, T., Gurfil, P. Long-term evolution of orbital inclination due to third-body inclination. *Celestial Mechanics and Dynamical Astronomy*, **2021**, 133(1): 1.

[12] Naoz, S., Farr, W. M., Lithwick, Y., Rasio, F. A., Teyssandier, J. Secular dynamics in hierarchical three-body systems. *Monthly Notices of the Royal Astronomical Society*, **2013**, 431(3): 2155–2171.

[13] Anderson, J. D., Lau, E. L., Sjogren, W. L., Schubert, G., Moore, W. B. Europa's differentiated internal structure: Inferences from two Galileo encounters. *Science*, **1997**, 276(5316): 1236–1239.

[14] Carbone, A., Cinelli, M., Circi, C., Ortore, E. Observing Mercury by a quasi-propellantless mission. *Celestial Mechanics and Dynamical Astronomy*, **2020**, 132: 8.

[15] Iess, L., Stevenson, D. J., Parisi, M., Hemingway, D., Jacobson, R. A., Lunine, J. I., Nimmo, F., Armstrong, J. W., Asmar, S. W., Ducci, M., *et al.* The gravity field and interior structure of Enceladus. *Science*, **2014**, 344(6179): 78–80.

Marco Cinelli received his Ph.D. degree in 2017 at Sapienza University of Rome, Italy. He is a research fellow at "Istituto di Astrofisica e Planetologia Spaziali" (IAPS) of the Italian National Institute for Astrophysics (INAF) in Rome. He is currently involved in the GALILEO for Science project (G4S) funded by the

Italian Space Agency (ASI) and aims to perform a set of measurements in the field of fundamental physics with the two Galileo satellites DORESA and MILENA. He is an adjunct professor at the Universitas Mercatorum of Rome, Italy. E-mail: marco.cinelli@inaf.it.

Hanlun Lei received his Ph.D. degree in astronomy from Nanjing University, China, in 2015. Currently, he is an associate professor at the School of Astronomy and Space Science in Nanjing University. his research interest focuses on astrodynamics and celestial mechanics, including space manifold dynamics as well as resonant dynamics of minor bodies in the solar system. E-mail: leihl@nju.edu.cn.

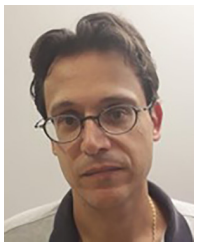

Emiliano Ortore graduated in aerospace engineering (M.S. degree) and in astronautical engineering and pursued his Ph.D. degree in aerospace engineering at Sapienza University of Rome, Italy. Since 2004, he has been working as a researcher at Sapienza University of Rome. Research fields include: celestial mechanics; orbits and satellite constellations for the Earth observation, telecommunication, and navigation; orbits for the observation of planets, moons, and asteroids; and remote sensing applications. E-mail: emiliano.ortore@uniroma1.it.

Christian Circi is currently an associate professor in flight mechanics at the Department of Astronautical, Electrical, and Energy Engineering, Sapienza University of Rome, Italy. He received his M.S. degree in aeronautical engineering and aerospace engineering and his Ph.D. degree in aerospace engineering at Sapienza University of Rome. He worked as a researcher at the Grupo de Mecanica of Vuelo-Madrid (GMV) and a research assistant at the Department of Aerospace Engineering. He is a lecturer in "*Interplanetary Trajectories*" and "*Flight Mechanics of Launcher*" in the master degree course of space and astronautical engineering at Sapienza University of Rome. His principal research fields are third-body and solar perturbations, interplanetary and lunar trajectories, solar sails, orbits for planetary observation, and the ascent trajectory of Launcher. He is an associate editor for *Aerospace Science and Technology*, *International Journal of Aerospace Engineering*, and *Astrodynamics*. E-mail: christian.circi@uniroma1.it.